Journal of Energy Storage 30 (2020) 101557

Contents lists available at ScienceDirect

Journal of Energy Storage

journal homepage: www.elsevier.com/locate/est

Digital twin for battery systems: Cloud battery management system with online state-of-charge and state-of-health estimation

Weihan Li*[a,b], Monika Rentemeister[a,b], Julia Badeda[e], Dominik Jöst[a,b], Dominik Schulte[f], Dirk Uwe Sauer[a,b,c,d]

[a] Chair for Electrochemical Energy Conversion and Storage Systems, Institute for Power Electronics and Electrical Drives (ISEA), RWTH Aachen University, Jaegerstrasse 17/19, 52066 Aachen, Germany
[b] Juelich Aachen Research Alliance, JARA-Energy, Germany
[c] Institute for Power Generation and Storage Systems (PGS), E.ON ERC, RWTH Aachen University, Germany
[d] Helmholtz Institute Münster (HI MS), IEK-12, Forschungszentrum Jülich, Germany
[e] ABO Wind AG, Wiesbaden, Germany
[f] BatterieIngenieure GmbH, Aachen, Germany

ARTICLE INFO

Keywords:
Digital twin
Cloud computing
Internet of things
Battery management system
State of charge
State of health

ABSTRACT

Battery management is critical to enhancing the safety, reliability, and performance of the battery systems. This paper presents a cloud battery management system for battery systems to improve the computational power and data storage capability by cloud computing. With the Internet of Things, all battery relevant data are measured and transmitted to the cloud seamlessly, building up the digital twin for the battery system, where battery diagnostic algorithms evaluate the data and open the window into battery's charge and aging level. The application of equivalent circuit models in the digital twin for battery systems is explored with the development of cloud-suited state-of-charge and state-of-health estimation approaches. The proposed state-of-charge estimation with an adaptive extended H-infinity filter is robust and accurate for both lithium-ion and lead-acid batteries, even with a significant initialization error. Furthermore, a state-of-health estimation algorithm with particle swarm optimization is innovatively exploited to monitor both capacity fade and power fade of the battery during aging. The functionalities and stability of both hardware and software of the cloud battery management system are validated with prototypes under field operation and experimental validation for both stationary and mobile applications.

1. Introduction

With the rapid advances in energy storage technologies, the battery system has emerged as one of the most popular energy storage systems in stationary and mobile applications to reduce global carbon emissions [1]. However, without proper monitoring and controlling of the batteries by a battery management system (BMS), problems concerning safety, reliability, durability, and cost will appear. The state-of-the-art BMS includes two main modules: BMS-Master and BMS-Slave, which can be combined in one embedded system or designed as two separate systems with wiring communication [2]. While the BMS-Slave is responsible for monitoring the battery cells with signal acquisition and filtering, more advanced functions, such as battery diagnostic algorithms, which require high computation power, are implemented in the BMS-Master. However, with the increase in the number of battery cells and the scale of the battery systems, the reliability and cost of the wiring communication are becoming challenging.

As the most important functions of the BMS, accurate estimation of the state of charge (SOC) and the state of health (SOH) deliver essential information about the battery's charge level and aging level, which can be used to perform maintenance or adapt operational strategies to extend its service life. Due to the easy implementation and small computation power requirement, open-loop algorithms, e.g., Coulomb counting [3] and open-circuit voltage method [4], are used to estimate the battery's SOC. Considering the high dynamic operation load in mobile battery systems and the tendency of multi-use application of stationary battery systems [5], the significant accumulated error due to current sensor uncertainties and the rare appearance of relaxation status reduce the reliability of these open-loop algorithms. Compared with SOC estimation, SOH estimation is more challenging due to the

* Corresponding author at: Chair for Electrochemical Energy Conversion and Storage Systems, Institute for Power Electronics and Electrical Drives (ISEA), RWTH Aachen University, Jaegerstrasse 17/19, 52066 Aachen, Germany.
E-mail addresses: batteries@isea.rwth-aachen.de, weihan.li@isea.rwth-aachen.de (W. Li).

https://doi.org/10.1016/j.est.2020.101557
Received 2 April 2020; Received in revised form 2 May 2020; Accepted 15 May 2020
Available online 23 June 2020

complex nonlinear aging mechanisms of the batteries. Although Electrochemical Impedance Spectroscopy [6–8] is commonly applied offline to detect the aging levels of the batteries, the strict input-signal requirements are obstacles for their online application in a BMS. To achieve accurate battery state monitoring, different model-based approaches were developed for SOC [9–13] and SOH [14–16] estimation. However, with the increase of battery cell number and algorithm complexity, onboard BMS is faced with problems in computation power and data storage for precise estimation and prediction of the battery's states with model-based algorithms. Furthermore, new functionalities, such as aging prognostics and strategy optimization, which work based on historical operation data of the battery cells, are difficult to be implemented onboard.

To overcome these obstacles, BMS can be revolutionized by applying cloud computing [17] and the Internet of Things (IoT) [18] technologies. The computation and data storage capabilities increase exponentially, and all battery relevant data can be measured and transmitted seamlessly to the cloud platform, which is used to build up the digital twin [19] for battery systems. The digital twin can not only show the data measured by sensors in battery packs but also visualize the internal state of each battery cell with advanced diagnostic algorithms. With the collection of big data in one base, system prognostics and optimizations can be achieved by machine learning algorithms, which will revolutionize our understanding of battery aging. Furthermore, the system reliability increases by replacing wiring communication with wireless IoT communication. Compared with onboard BMSs, digital twin for battery systems has potential benefits in four aspects as follows, which all together contribute to the reduction of the total cost of ownership and the increase of system performance:

- Monitoring and diagnostics
  Continurous and accurate monitoring of the battery state with advanced diagnostic algorithms, supported by high computation power.
- Lifetime prognostics
  Accurate prediction of the degradation trend with machine learning based on full life-cycle operation data.
- Fault detection and prediction
  Early detection of system faults in different levels with big data analysis, increasing the system safety and reliability.
- Evaluation and optimization
  Optimization of the system design and operation strategy by evaluating the big data from battery systems with different operation scenarios.

The pioneering work has shown several concepts to apply cloud computing and IoT in BMS for both stationary and mobile battery systems [20–22]. Tanizawa et al. [20] proposed a cloud system for electric vehicles to manage the battery information in the battery replacement system. Harish et al. [21] proposed a battery monitoring system based on IoT for batteries in a microgrid system. Most recently, Kim et al. [22] proposed a cloud-based battery condition monitoring and fault diagnosis platform for large-scale stationary battery systems. However, the works mentioned above suffer from two major drawbacks awaiting further improvements. Firstly, the technical details of both software and hardware design of the cloud BMS were rarely introduced, and the functionalities of the system have not been validated with field operation. Secondly, cloud-suited battery diagnostic algorithms are missing, which can improve the diagnostic accuracy and benefit from the high computation power and data storage capability of the cloud BMS.

This paper aims to bridge the aforementioned research gap and proposes a cloud BMS to build up the digital twin for battery systems, releasing the computation and data storage limitations of the onboard BMS. The information of the batteries connected with the cloud can be shared by the proposed IoT component, enabling the seamless data communication among individual battery systems and the digital twin. Moreover, the proposed model-based battery diagnostic algorithms with adaptive extended H-infinity filter (AEHF) and particle swarm optimization (PSO) for SOC and SOH estimation, are implemented in the cloud BMS, ensuring continuous and accurate monitoring of the battery state with the digital twin. The AEHF algorithm based on the extended Thevenin model provides a robust approach for SOC estimation. The PSO-based algorithm estimates all the parameters of the extended Thevenin model, providing both information of the battery's capacity fade and power fade synchronously. Furthermore, two prototypes of the cloud BMS are designed and produced for both the field test of the system's functionalities and experimental test of the cloud-suited battery diagnostic algorithms with two different battery technologies, i.e., lithium-ion and lead-acid batteries.

We begin in Section 2 by introducing the operation principles of the cloud BMS and the technical details of the subsystems. Battery modeling is presented in Section 3. In Sections 4 and 5, the model-based SOC estimation approach with the AEHF algorithm and SOH estimation approach with the PSO algorithm are introduced, respectively. In Sections 6 and 7, the experimental set-up and validation results of both cloud-BMS functionalities and cloud-suited battery diagnostic algorithms are discussed. Section 8 draws the conclusions and points towards future work.

2. Cloud battery management system

By bridging the physical and the virtual world, digital twin allows the virtual entity to the battery systems simultaneously with the seamless transmission of data. Compared with the onboard BMS, the cloud BMS has advantages in both hardware and software, as summarized in Table 1. In terms of hardware, the cloud BMS has high computation power, enormous data storage capability, and high system reliability. These features further support the application of advanced algorithms in software. On the one hand, the performance of the functions, which already exist in onboard BMSs, can be further improved with more advanced algorithms. On the other hand, new functions, such as data-based lifetime prediction and system optimization, which are hard to be implemented in onboard BMSs, can be implemented in the cloud. In this section, operation principles of the cloud BMS and the functionalities of the subsystems are introduced, as depicted in Fig. 1.

2.1. Stationary and mobile battery systems

In electricity systems with a high penetration of renewable energy generation, such as solar and wind energy, stationary battery systems can be used to balance the power supply. High costs and single applications make the stationary battery systems operating under inefficient scenarios. To use the energy of the UPS systems efficiently, Badeda et al. [5] looked into multi-use applications by delivering additional services, e.g., peak shaving and primary containment reserve. Compared with the batteries in single applications, multi-use battery systems need continuous real-time state monitoring and diagnostics to ensure the availability of power for different use cases, highlighting the benefits of the cloud BMS.

With the electrification of vehicles, battery systems are playing an

Table 1
Summary of the advantages of cloud BMS.

	Advantages
Hardware	High computation power Enormous data storage capability High system reliability
Software	Accurate monitoring and diagnostics Reliable prognostics and optimization

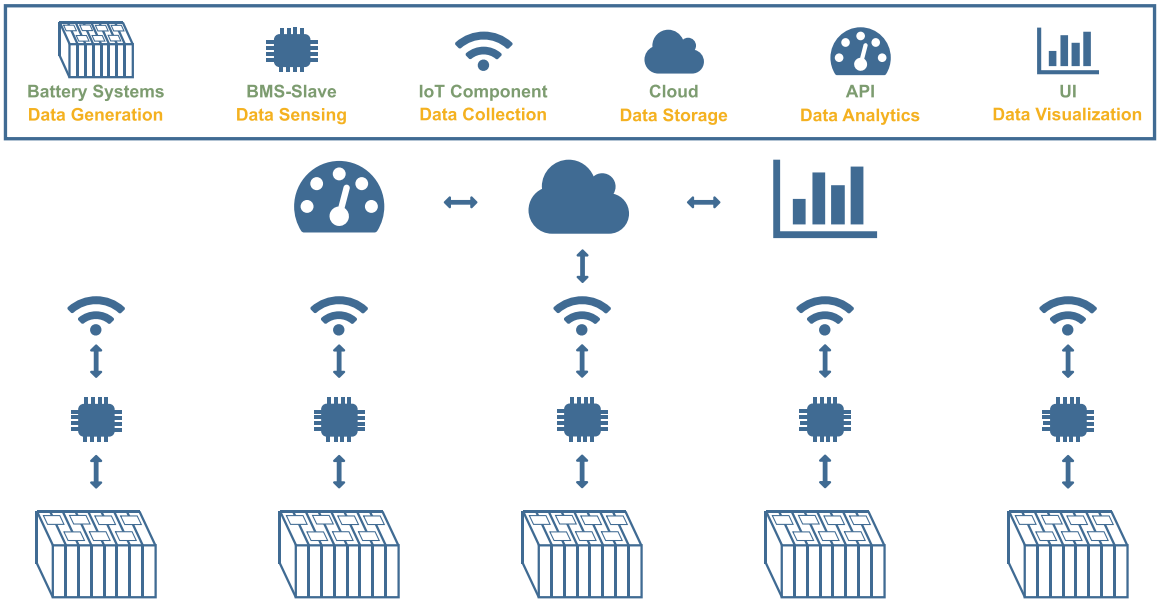

Fig. 1. Schematic of the cloud BMS, which consists of six subsystems: the battery systems for data generation, the BMS-Slave for data sensing, IoT component for data collection, cloud for data storage, application programming interface (API) for data analytics and user interface (UI) for data visualization.

essential role in the energy storage of electric vehicles. Compared with the stationary battery systems, the batteries in mobile applications are usually working with a larger depth of discharge (DOD) and under more dynamic conditions, which in turn require more advanced algorithms for battery diagnostics, prognostics, and optimization. With the emerging new communication technologies, e.g., 5G technology, the mobile battery systems can be connected with the cloud by the proposed cloud BMS, reducing battery aging and improving the battery's safety, reliability and performance. The data generated by stationary and mobile battery systems contain a wealth of information about the operation history, which can be analyzed with the digital twin to adapt the operation strategy to extend service life.

2.2. BMS-Slave

The main components in the developed BMS-Slave for data sensing are multi-cell battery monitors LTC 6804G-2 and LPC 11C14F/301. The LTC measures up to 12 battery cells connected in series with a total measurement error of less than 1.2 mV, which can also be connected in series to monitor high-voltage battery strings. The LPC is a 32-bit ARM Cortex-M0 based microcontroller, which sends the measurement commands to the LTC and receives the measured data in hexadecimal values from the LTC. The BMS-Slave performs data acquisition by measuring the voltage, current, and temperature of the battery cells with sensors at different sampling rates.

2.3. IoT Component

The basic idea behind IoT is to make the devices, i.e., the stationary and mobile battery systems embedded with electronics and connected with the internet, communicate and interact with others to be monitored and controlled remotely. Therefore, a stable internet connection is vital for a stable real-time data transfer between the battery system and the digital twin. In order to increase the reliability of the whole system, the functions which are required at each time point during operation should also run locally, guaranteeing the system safety. An advanced version of these functions will run in the cloud with advanced algorithms, which provide higher accuracy while requiring high computation power. The functions which require historical operation data can only run in the cloud. The digital twin will communicate with the battery system and update the model parameters to improve the system performance and restrain battery degradation.

Considering the advantages of Raspberry Pi as a single-board computer with relatively low price and weight, it is responsible for collecting data from the batteries and communicating with the cloud platform and other battery systems. The measured data of the battery cells are sent to the IoT component by the BMS-Slave based on the Controller Area Network (CAN) protocol. The software programs were developed and implemented with Python in the IoT component to translate the CAN signals into physical values. Furthermore, the IoT component is also responsible for sending the generated data to the cloud under TCP/IP and Message Queuing Telemetry Transport (MQTT) protocol with the assured security and privacy.

2.4. Cloud

As IoT devices usually have limited storage and computation capabilities and do not allow complex data processing, cloud computing with virtually unlimited storage capability and processing power enables the scalable and real-time data analysis of the IoT devices. The proposed cloud platform in the cloud BMS consists of a data logger and a database hosted in Germany. The data logger captures a massive amount of non-structured or semi-structured data produced by the battery systems and enables a secure gateway and data transfer into the cloud database, which was extensively certified and has distributed denial-of-service (DDoS) protection and multi-redundant connections. Only the owners and operators of the battery systems have access to the data, and data privacy and security are guaranteed.

2.5. Application programming interface

As a part of the cloud BMS, Application Programming Interface (API) is the bridge between the cloud database and the data-analytic algorithms, which offers several popular programming languages, such as Matlab and Python. With the proposed API, the state of the battery cells in each battery pack can be monitored using battery diagnostic algorithms based on different battery models. Digital twin for the battery packs can therefore show the accurate state of each battery cell in real-time, e.g., SOC and SOH, which will be introduced in Section 4 and 5. Furthermore, the field data collected from different battery systems

can be used for accurate predictions and system optimization, reducing the wear and tear on the batteries through the adaption of battery management, which will not be introduced in detail in this work.

2.6. User interface

User Interface (UI), which is the belt between the cloud platform and the battery system operators, is responsible for inspecting and visualizing the digital twin. Compared with the onboard BMS which has little data visualization opportunities, the browser-based UI in our cloud BMS can provide not only the real-time visualization of the measurement data and internal states of the battery cells but also historical operation data with numerous display types and options, which helps the operators in scheduling maintenance and repair. With different kinds of alarm functions, which can be set up for the original and virtual data points, the operators can be informed by the UI as soon as the fault of the systems is identified, increasing the chances of preventing damaging effects and thus improving the system reliability and reducing the maintenance cost. In order to protect the data, the UI endpoints are accessible only via HTTPS and require user authentication.

3. Battery modeling

Considering the functionalities of the digital twin for battery systems, modeling of the battery dynamics is of vital importance, which is the basis for accurate battery diagnostics. There are three main categories of models for battery cells: equivalent circuit models (ECMs) [25], electrochemical models [26–28], and machine learning models [29–32]. In our opinion, all these models have highlights and limitations and will play different roles in the digital twin for battery systems. In this work, we focus on the application of ECMs in the digital twin for accurate monitoring of SOC and SOH of the battery cells.

The numerous ECMs, such as R_{int} model, Thevenin model, and nth RC networks model, have attracted a lot of interest in past years for real-time battery state estimation. These models use electrical circuit components, such as resistances, capacitances, and voltage sources, to mimic the dynamic response of a battery. Considering the balance between model accuracy and computation time, an extended Thevenin model, as shown in Fig. 2, is proposed in this paper to model the battery dynamics, which can be expressed as follows:

$$\dot{U}_1 = -\frac{U_1}{R_1 C_1} + \frac{I}{C_1} \tag{1}$$

$$\dot{U}_2 = -\frac{U_2}{R_2 C_2} + \frac{I}{C_2} \tag{2}$$

$$U_t = U_{oc} - U_1 - U_2 - IR_0 \tag{3}$$

where I denotes the input current, U_t denotes the terminal voltage, U_{oc} denotes the open-circuit voltage which has a nonlinear relationship with battery SOC, R_0 is the ohmic resistance, $R_{1,2}$ and $C_{1,2}$ are resistances and capacitances for the two RC-circuits, and $U_{1,2}$ are voltage drops over $R_{1,2}$. Based on the extended Thevenin model, state estimation and parameter identification algorithms will be introduced in the following sections to estimate the SOC and SOH of the battery in the digital twin.

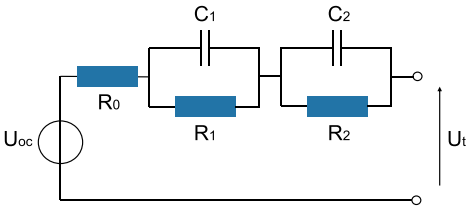

Fig. 2. Schematic of the extended Thevenin model.

4. State-of-charge estimation with adaptive extended H-infinity filter

4.1. Adaptive extended H-infinity filter

H-infinity filters have shown high robustness and are further explored in battery state estimation [12]. The adaptive extended H-infinity filter (AEHF) is an optimal estimator, which can be computed recursively using noisy input data in real-time to analyze and solve a wide class of state estimation problems. Zhang et al. [12] applied AEHF to estimate the SOC of the lithium-ion battery and the AEHF has shown its advantage compared with the Kalman filters considering the uncertainty in battery dynamic models and noise statistics. Considering the discrete-time model of a general nonlinear system in a state-space form, we have

$$x_{k+1} = Ax_k + Bu_k + w_k \tag{4}$$

$$y_k = Cx_k + Du_k + v_k \tag{5}$$

where u_k and y_k represent the system inputs and outputs, x_k denotes the system states, w_k and v_k are the system process noise and measurement noise, the matrices A_k, B_k, C_k, and D_k describe the system dynamics.

The aim of H-infinity filters is to estimate the states $z_k = L_k x_k$ by applying the game theory and to improve the algorithm robustness by estimating the covariance values using the covariance matching technique [11]. If x_k are states to be estimated, then L_k is an identity matrix. The implementation flowchart of AEHF for processing state estimation is depicted in Fig. 3. The realization of the AEHF is divided into three sub-processes and is detailed as below.

4.1.1. Estimation process

In this process, the estimation of the states and outputs of the system are updated. The prior state estimation $\hat{x}_k^-$ and error covariance P_k^- are calculated by

$$\hat{x}_k^- = A_{k-1}\hat{x}_{k-1}^+ B_{k-1} \tag{6}$$

$$P_k^- = A_{k-1}P_{k-1}A_{k-1}^\top + Q_{k-1} \tag{7}$$

where Q_{k-1} is the weighting matrix. Afterward, the observer stability criteria are checked by

$$(P_k^-)^{-1} - \theta_k^{-2} L_k^\top L_k > 0 \tag{8}$$

where θ_k is the tuning parameter. Furthermore, the gain matrices are updated as follows:

$$R_{e,k} = \begin{bmatrix} R_{k-1} & 0 \\ 0 & -\theta_k^2 I \end{bmatrix} + \begin{bmatrix} C_k \\ L_k \end{bmatrix} P_k^- \begin{bmatrix} C_k^\top & L_k^\top \end{bmatrix} \tag{9}$$

$$H_k = P_k^- \begin{bmatrix} C_k^\top & L_k^\top \end{bmatrix} R_{e,k}^{-1} \tag{10}$$

$$H_{s,k} = P_k^- C_k^\top (R_{k-1} + C_k P_k^- C_k^\top)^{-1} \tag{11}$$

where $R_{e,k}$ and $H_{s,k}$ are transition matrices and H_k is the H-infinity

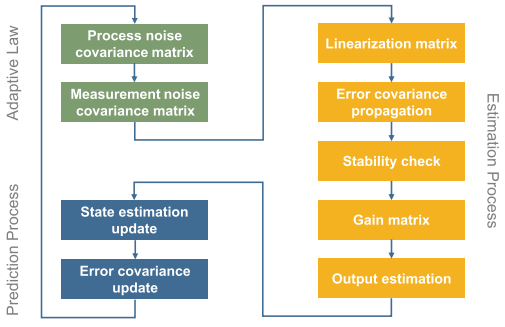

Fig. 3. Implementation flowchart of the adaptive extended H-infinity filter.

matrix. The estimation of the system output $\hat{y}_k$ is provided by

$$\hat{y}_k = C\hat{x}_k^- + Du_k + v_k. \tag{12}$$

4.1.2. Prediction process

In the prediction process, the state and error covariance matrix for the next time step is calculated by

$$\hat{x}_{k+1} = A\hat{x}_k + Bu_k + H_k e_k \tag{13}$$

$$P_k = \left(I - H_k \begin{bmatrix} C_k \\ L_k \end{bmatrix}\right) P_k^- \tag{14}$$

where e_k represents the output estimation error as follows:

$$e_k = y_k - \hat{y}_k. \tag{15}$$

4.1.3. Adaptive process

The tuning parameter θ_k and the weighting matrices Q_k and R_k play important roles in H infinity filters and are adjusted in each time step as follows:

$$\theta_k = \alpha\sqrt{\max(\mathrm{eig}(P_k^-))} \tag{16}$$

$$R_k = \frac{1}{N}\sum_{j=k-N+1}^{k}(e_j e_j^\top - C_j P_j C_j^\top) \tag{17}$$

$$Q_k = \frac{1}{N}\sum_{j=k-N+1}^{k}(H_{s,k} e_k e_j^\top H_{s,j}^\top - A_{j-1} P_{j-1} A_{j-1}^\top). \tag{18}$$

4.2. SOC Estimation with AEHF

The SOC of the battery is defined as the ratio of the present charge to the nominal battery capacity C_N, given by

$$\mathrm{SOC}_t = \mathrm{SOC}_0 - \frac{1}{C_N}\int_{t_0}^{t}\eta I dt \tag{19}$$

where SOC_t and SOC_0 are the SOC of the battery at initial time t_0 and current time t, respectively, η is the Coulomb efficiency, and I denotes the current flowing through the voltage source. With the transformation of (1)–(3) and (19) into a discrete-time system, the input matrix u_k, output matrix y_k and the state matrix x_k as shown in (4) and (5), are defined as follows:

$$u_k = I_k \tag{20}$$

$$y_k = U_{t,k} \tag{21}$$

$$x_k = [\mathrm{SoC}_k \quad U_{1,k} \quad U_{2,k}]^\top. \tag{22}$$

The parameter matrices A_k, B_k, C_k and D_k are defined by

$$A_k = \begin{bmatrix} 1 & 0 & 0 \\ 0 & \exp\left(\frac{-\Delta t}{R_1 C_1}\right) & 0 \\ 0 & 0 & \exp\left(\frac{-\Delta t}{R_1 C_1}\right) \end{bmatrix} \tag{23}$$

$$B_k = \begin{bmatrix} \frac{\eta\Delta t}{C_N} \\ R_1\left(1 - \exp\left(-\frac{-\Delta t}{R_1 C_1}\right)\right) \\ R_2\left(1 - \exp\left(-\frac{-\Delta t}{R_2 C_2}\right)\right) \end{bmatrix} \tag{24}$$

$$C_k = \left[\frac{dU_{oc,k}(\mathrm{SOC})}{d\mathrm{SOC}}\Big|_{\hat{\mathrm{SOC}}_k} \quad -1 \quad -1\right] \tag{25}$$

$$D_k = [-R_0] \tag{26}$$

where $U_{oc,k}(\mathrm{SOC})$ represents the nonlinearity between SOC and U_{oc}, which can be measured with experiments. The measurement and identification of the parameters in the parameter matrices will be introduced in the next sections.

With the definitions of the system states and parameter matrices in (20)–(26), AEHF described with (6)–(18) can be applied to estimate the SOC of the battery.

5. State-of-health estimation with particle swarm optimization

5.1. Particle swarm optimization

As a branch of Artificial Intelligence (AI), PSO is a meta-heuristic algorithm initially inspired by the choreography of a bird flock [23]. It can optimize a numeric problem by simulating the behaviors of swarms. PSO and its variants are becoming quite popular due to their high convergence rate and robustness. They are explored and utilized to optimize the nonlinear system parameters [16]. The main steps of PSO are summarized as follows.

5.1.1. Random initialization

The positions x_i and velocities v_i of all the particles are generated and initialized randomly, the dimensions of which are depending on the number of the parameters to be optimized.

5.1.2. Swarm evolution

At each iteration, each particle in the swarm is improved by two values, namely P_{best}, and G_{best}. P_{best} represents the best solution in all previous generations of each particle and G_{best} represents the best solution of all the particles in previous generations, also called the best global solution. Each particle updates its location x_i and velocity v_i by

$$x_{i+1} = v_{i+1} + x_i \tag{27}$$

$$v_{i+1} = wv_i + c_1 r_1(P_{best} - x_i) + c_2 r_2(G_{best} - x_i) \tag{28}$$

where $c_{1,2}$ are learning rates influencing the algorithm convergence performance, w is the inertia weighting factor, $r_{1,2}$ are random values between 0 and 1. After updating the positions and velocities, the fitness function is evaluated for each particle to update the P_{best} and G_{best}. The iterated optimization process will stop when the predefined fitness value or the maximum iteration number is reached. The implementation flowchart of applying PSO for parameter identification is depicted in Fig. 4.

5.2. SOH Estimation with PSO

The SOH of the battery is a metric to indicate the battery's aging level. The commonly used SOH indices can be divided into two groups: capacity fade indices and power fade indices [24]. With battery aging, the value of the remaining capacity of the battery will decrease because of the capacity loss mechanisms, resulting in the capacity fade of the battery. Meanwhile, the value of ohmic resistance and polarization

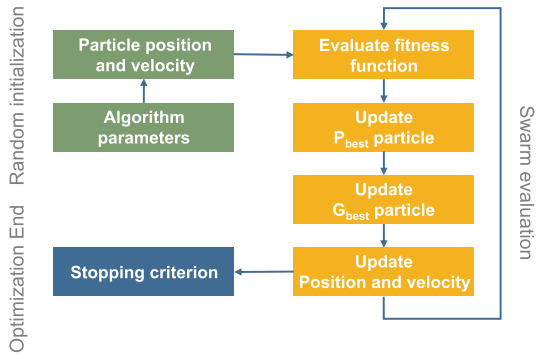

Fig. 4. Implementation flowchart of the particle swarm optimization.

resistances will increase, resulting in the power fade of the battery. In this work, the SOH indicating the battery's capacity fade, SOH_C, and the SOH indicating the battery's power fade, SOH_R, are determined by PSO synchronously.

The SOH_C of the battery is usually defined as follows:

$$SOH_{C,t} = \frac{C_{N,t}}{C_{N,0}} \tag{29}$$

where $C_{N,0}$ and $C_{N,t}$ are the nominal capacity and the remaining capacity at current time t. The SOH_R of the battery is determined from the ohmic resistance increasing, namely

$$SOH_{R,t} = \frac{R_{0,t}}{R_{0,0}} \tag{30}$$

where $R_{0,0}$ and $R_{0,t}$ are the ohmic resistance at battery's begin of life (BoL) and current time t. It is worthy of notifying that the identification of the aging level of the battery based on the increase of the resistances R_1 and R_2 can also be implemented, which will not be introduced in detail in this work. The OCV curve is assumed to be unchanged during aging and the update of OCV curve is considered outside the scope of this work and will be investigated in the future. The End of Life (EoL) of the battery regarding the capacity fade is reached when the value of $SOH_{C,t}$, as shown in (29), equals to 80%. However, the EoL can also be defined as the time that the value of the ohmic resistance increases 30%, i.e., the value of $SOH_{R,t}$ reaches 130%, considering the battery's power fade, as shown in (30). Therefore, it is essential to estimate both $SOH_{C,t}$ and $SOH_{R,t}$ at the same time, which were not provided by most of the literature.

The ECM parameters, such as nominal capacity C_N, resistances $R_{0,1,2}$, and capacitances $C_{1,2}$, can be identified based on the measurement data of current and voltage with PSO according to the fitness function F as follows:

$$F = \frac{1}{N}\sum_{i=1}^{N}\left(U_{t,i} - \hat{U}_{t,i}\right)^2 \tag{31}$$

where N is the total number of the data points, $U_{t,i}$ is the measured battery terminal voltage, $\hat{U}_{t,i}$ is the estimated battery terminal voltage with the identified parameters. The PSO will stop the optimization process when the values of the estimated parameters converge. The identified C_N and R_0 in the final G_{best} are then used to calculate the SOH_C and SOH_R of the battery in (29) and (30).

Considering that the aging mechanism is slower compared to the SOC change, the parameter identification with PSO was designed to run in the cloud based on a period of field data. The identified parameters C_N, $R_{0,1,2}$, and $C_{1,2}$ can not only be used to estimate the battery's SOH but also be injected back into SOC algorithms to improve the estimation accuracy with accurate model parameters. Fig. 5 presents a strategy in which the SOC and SOH estimation can be implemented together online.

6. Experimental set-up

To validate the functionalities and stability of both hardware and software, we designed and produced two prototypes of the proposed

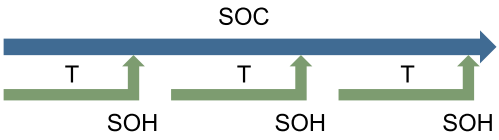

Fig. 5. Implementation strategy of AEHF-based SOC estimation and PSO-based SOH estimation. The AEHF will run continuously for all time. The battery parameters and SOH are updated after each period of T by running the PSO based on the field data in the previous period. This process is repeated for the whole duration of use.

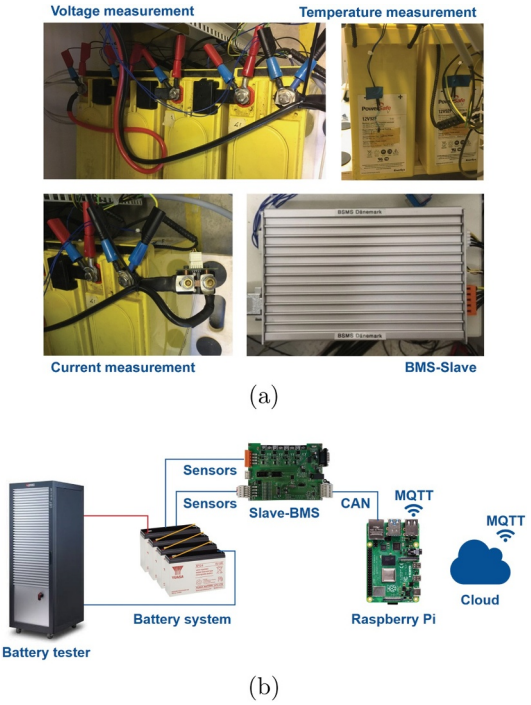

Fig. 6. (a) UPS system connected with the cloud BMS prototype A. (b) Battery test bench for lithium-ion and lead-acid batteries connected with the cloud BMS prototype B to validate the proposed SOC and SOH algorithms.

cloud BMS. As the dominating battery technology nowadays for the UPS market is the lead-acid battery, a UPS system consisting of lead-acid batteries was chosen to validate the monitoring functionalities of the cloud BMS. Furthermore, the proposed cloud-suited battery diagnostic algorithms were validated with different battery technologies, i.e., lithium-ion battery and lead-acid battery, considering the increasing market share of lithium-ion batteries and application potential of the cloud BMS in mobile battery systems, e.g., electric vehicles.

6.1. Field validation of the cloud BMS functionalities

The prototype A of the cloud BMS was connected with a UPS system in Denmark, as shown in Fig. 6(a). The battery system consists of four 12 V, 92 Ah Hawker Enersys AGM lead-acid batteries connected in series, as summarized in Table 2. The UPS system was under operation and kept at float charge. The voltage and temperature of four batteries were measured and transmitted to the cloud and monitored in Germany remotely with the developed UI in real-time to validate the performance of the system hardware.

6.2. Experimental validation of the AEHF-based SOC estimation algorithm

To validate the proposed AEHF-based SOC estimation algorithm experimentally, we installed prototype B of the cloud BMS on batteries with different chemistries in our laboratory in Germany. The lead-acid batteries and lithium-ion batteries were applied to verify the accuracy and stability of the algorithm in multi-use stationary battery systems and mobile battery systems, respectively.

The stationary battery system is composed of four 12 V, 7 Ah Yuasa AGM lead-acid batteries, as summarized in Table 2, connected in series. This 48 V battery system was connected with a Digatron battery tester with 100 V, 50 A test circuits, as shown in Fig. 6(b). To validate the proposed AEHF-based SOC estimation algorithm for the mobile application, a lithium-ion battery, Samsung INR18650-35e, was connected with a Digatron battery tester with 5 V, 20 A test circuit and tested in a temperature chamber. The cathode and anode material of the lithium-

Table 2
Specifications of the batteries for experimental validations of the cloud BMS.

	Hawker Enersys	Yuasa NP7-12	Samsung INR18650-35e
Chemistry	Lead-acid	Lead-acid	Lithium-ion
Capacity [Ah]	92	7	3.40
Norminal voltage [V]	12	12	3.60
Cell dimension [mm]	395 × 105 × 264	151 × 65 × 94	65.25 × 18.55
Weight [kg]	27.60	2.20	0.05

ion battery is Lithium-Nickel-Cobalt-Aluminium-Oxide (NCA) and graphite, respectively. The specifications of the battery are summarized in Table 2. Before the validation test of the cloud-suited diagnostic algorithms, battery characterization tests, e.g., capacity tests and OCV tests were conducted for both batteries. During the OCV tests, the relaxation voltage of the battery under different SOC levels were measured. The average of OCVs in charging and discharging process were used as the OCV curve for the battery, reducing the influence of the hysteresis.

Considering the multi-use tendency of the stationary battery systems, we applied a dynamic current profile consisting of charging and discharging current pulses with amplitudes from 1 A to 5 A to validate the proposed SOC estimation algorithm with the lead-acid battery, as shown in Fig. 7(a). In contrast, a real-world driving data-based test profile was applied to the lithium-ion battery considering its high demand in automotive battery systems. As shown in Fig. 7(b), the maximum discharging and charging current of the test profile is 2 A and 9.6 A, respectively.

6.3. Experimental validation of the PSO-based SOH estimation algorithm

To validate the PSO-based SOH estimation algorithm, we carried out aging tests to age the same lithium-ion battery as introduced in Section 6.2. Cycling of the battery was conducted at a constant temperature of 25°C. In each aging cycle, the battery was discharged with the real-world driving data-based test profile, as depicted in Fig. 7(b), from 90% to 10% SOC. Then the battery was charged with 0.33 C constant current from 10% SOC back to 90% SOC. After every 30 aging cycles, a characterization test consisting of a pulse test and a capacity test was conducted at 25°C, as shown in Fig. 8. Within the multi-pulse test, a dynamic profile consisting of multi 10 s charging and discharging pulses at three different SOC levels, i.e., 80%, 50%, and 20%, with 0.5 C, 1 C, and 2 C was conducted. After that, the battery cell was discharged and charged under a capacity test with a constant current of 0.33 C between its cut-off voltages. The variance of the temperature does influence the value of the battery parameters, e.g., C_N, $R_{0,1,2}$, and $C_{1,2}$. This temperature relationship can be modeled by parameterizing the battery model under the same aging level with different temperatures, which is considered outside the scope of this work.

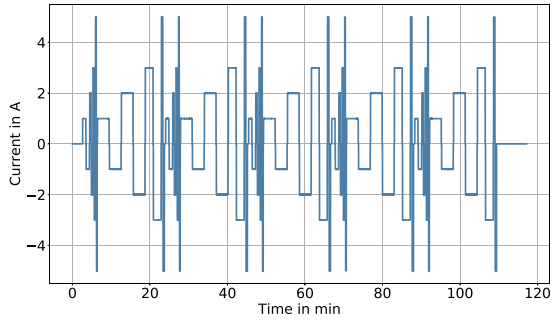

(a)

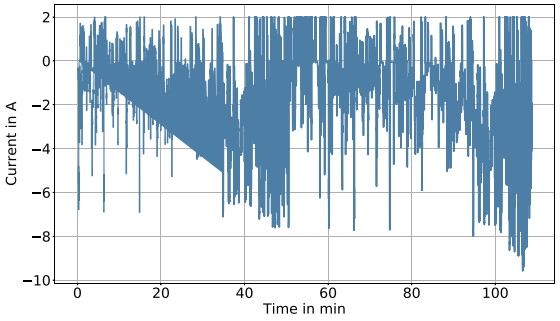

(b)

Fig. 7. Current profile for experimental validation of the AEHF-based SOC estimation algorithm. (a) Dynamic pulse profile for a multi-use stationary battery system. (b) Real-world driving data-based current profile for the mobile battery system.

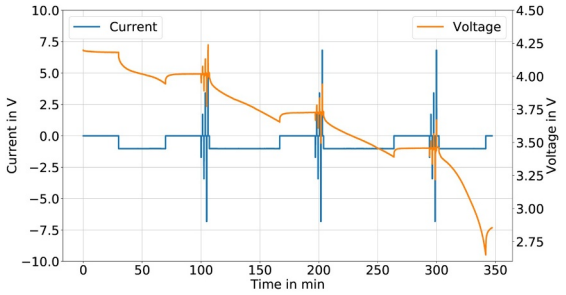

(a)

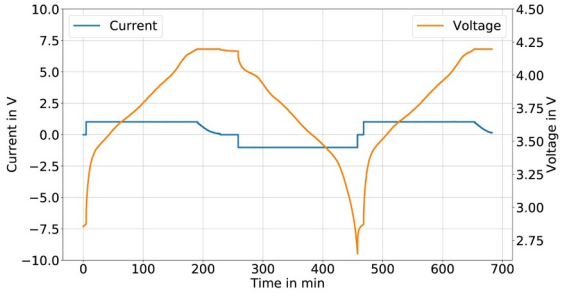

(b)

Fig. 8. Characterization test in the cyclic aging test. (a) Pulse test with 0.5 C, 1 C, and 2 C at 80% SOC, 50% SOC, and 20% SOC. (b) Capacity test with 0.33 C.

7. Results and discussions

7.1. Field validation of the cloud BMS functionalities

The validation results of the cloud BMS functionalities, as proposed in Section 2, are depicted in Fig. 9, where about 160 h of the voltage and temperature measurement data with the cloud BMS are visualized

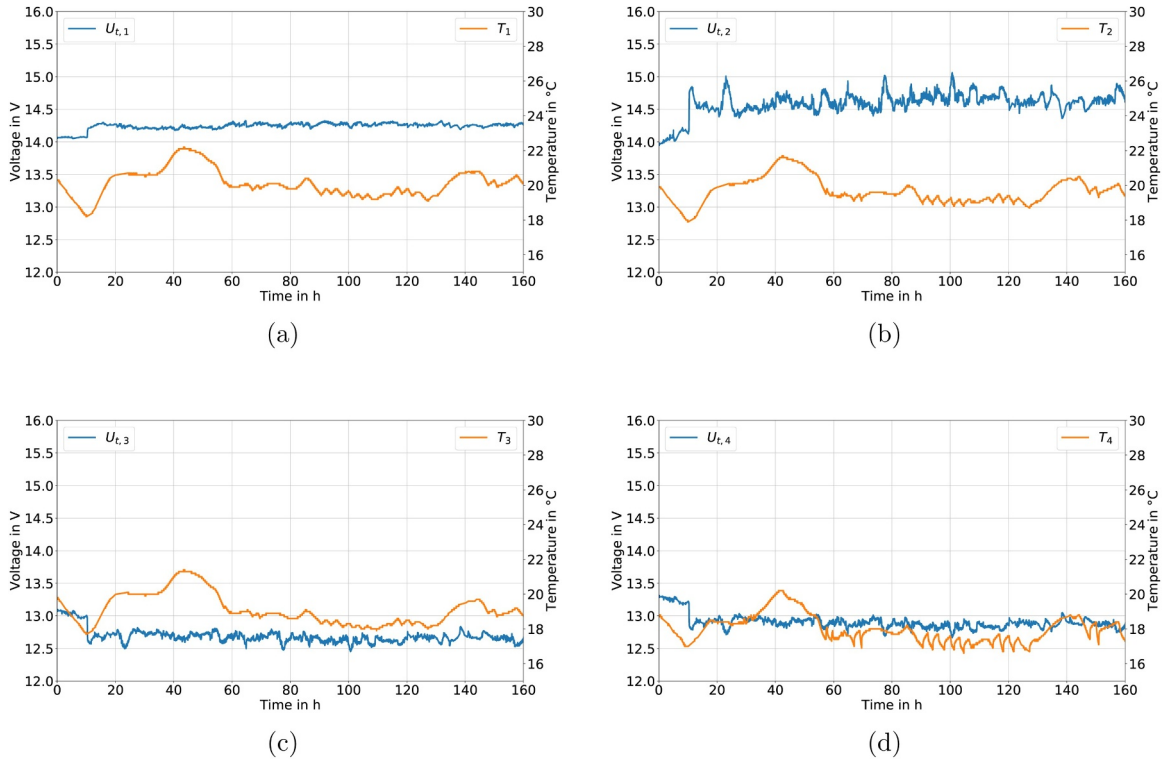

Fig. 9. Field data collected from the UPS with the cloud BMS in Denmark and monitored with the UI in Germany remotely. Voltage and temperature data of (a) battery 1, (b) battery 2, (c) battery 3, and (d) battery 4.

with the UI. The data were collected continuously, and the sensors have caught the variation of voltage and temperature of each battery in the system. The real-time remote monitoring of the battery system with the cloud BMS prototype A was verified.

Within the field validation of the cloud BMS, the hardware of the system, consisting of the BMS-Slave, the IoT component and the data logger in the cloud were working together with the proposed system's software, successfully verifying the functionalities of the cloud BMS, e.g., data sensing, data collection, data storage, and data visualization. The cloud BMS enables direct and real-time visualization and monitoring capability of large scale battery systems for the users and battery experts, which can also be adapted with new communication technologies, e.g., 5G technology, for the mobile battery systems, reducing the battery aging and improving the battery's safety, reliability and performance.

7.2. Experimental validation of the AEHF-based SOC estimation algorithm

The validation results of the AEHF-based SOC estimation algorithm, as proposed in Section 4, are depicted in Fig. 10. While the real voltage value was measured directly, the reference value of SOC was calculated by Coulomb counting with high-accuracy current sensors of battery tester with accurate SOC initial value.

The validation results for the lead-acid battery are shown in Fig. 10(a), (b), and (c). To check the self-regulation ability and the stability of the SOC algorithm, we applied an erroneous initial value of SOC to the cloud BMS. Both voltage estimation and SOC estimation can converge to the real value very fast. With a relatively long operation period, the voltage and SOC estimation can always follow the reference value of the battery with mean absolute error (MAE) of 0.01 V and 0.06%. The validation results for the lithium-ion battery under a real-world driving cycle are depicted in Fig. 10(d), (e), and (f). Similarly, an erroneous initial value of SOC was applied to check the self-regulation ability and stability of the algorithm for the lithium-ion battery. Both the estimation of voltage and SOC converged fast to the reference value. Within 90% DOD range, the voltage and SOC estimation of the lithium-ion battery can always match with the reference values with MAE of 0.01 V and 0.49%, respectively. The validation results show that the proposed AEHF-based SOC estimation algorithm is accurate and stable for both lead-acid and lithium-ion batteries in stationary and mobile application scenarios.

7.3. Experimental validation of the PSO-based SOH estimation algorithm

The validation results of the PSO-based SOH estimation algorithm, as proposed in Section 5, are presented in Fig. 11. The results of the parameter identification for the battery at BoL are visualized as an example in Fig. 11(a), (b), (c), and (d).

With the identified battery parameters, e.g., C_N, $R_{0,1,2}$, and $C_{1,2}$, identified by the proposed PSO approach, the extended Thevenin model is able to estimate the voltage of the battery accurately with the maximum absolute error of 0.11 V as shown in Fig. 11(a) and (b), indicating the accuracy of the parameter identification. As shown in Fig. 11(c), the fitness value, as described in (31), decreased very fast with the increase of the iteration number and converged to the minimum value within 600 iterations. This phenomenon indicates that the PSO-based algorithm is working to adapt the parameter values within the parameter boundaries to reduce the error between the measured and modeled voltage of the cell. The capacity of the battery $C_{N,t}$ also converged fast to a stable value within 600 iterations, as shown in Fig. 11(d). Meanwhile, the ohmic resistance $R_{0,t}$ of the battery, which is used in this work as an index for the power fade, also showed a fast convergence performance. The final estimated values of C_N and R_0 are 3.43 Ah and 27.2 mΩ, respectively.

Based on the real-world driving data, as shown in Fig. 7, the cell parameters, i.e., C_N and R_0, are identified with the proposed PSO-based algorithm at 19 different aging status within 540 aging cycles. As a benchmarking for the capacity estimation, the measured capacity of the battery with Coulomb counting under 0.33 C discharging was calculated as C_C from the characterization tests. The measured capacity C_C

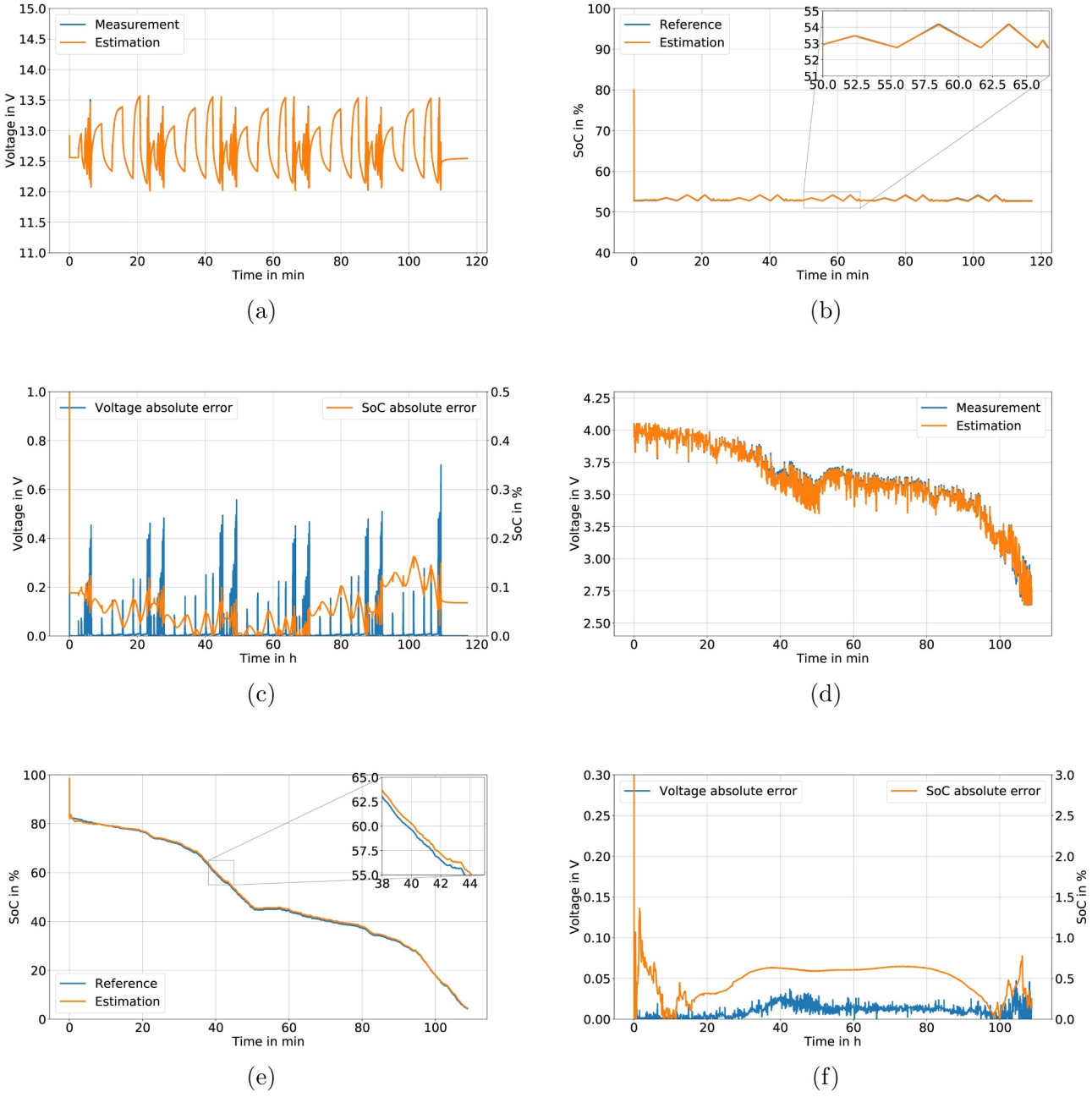

Fig. 10. Validation results of the AEHF-based SOC estimation algorithm with a lead-acid battery and a lithium-ion battery. (a) Validation results of the voltage estimation for the lead-acid battery. (b) Validation results of the SOC estimation for the lead-acid battery. (c) The absolute error of voltage and SOC estimation for the lead-acid battery. (d) Validation results of the voltage estimation for the lithium-ion battery. (e) Validation results of the SOC estimation for the lithium-ion battery. (f) The absolute error of voltage and SOC estimation for the lithium-ion battery.

and estimated capacity C_N at 19 different aging status are summarized in Table 3. According to (29), the measured and estimated SOH_C are depicted in Fig. 11(e). It is clear that the SOH_C of the battery decreased continuously from 1 to 0.89 within 520 aging cycles, indicating the capacity fade of the battery. The estimated SOH_C matches with the measured SOH_C with MAE of 0.74%.

Similarly, the ohmic resistance of the battery under 2 C current pulse at 80% SOC was calculated as R_C from the characterization tests for benchmarking. The measured ohmic resistance R_C and estimated ohmic resistance R_0 at 19 different aging status are summarized in Table 4. Both R_C and R_0 show the same increasing trend during cell aging. According to (30), the measured and estimated SOH_R are depicted in Fig. 11(f). The SOH_R of the battery increased from 1 to 1.25 within 520 aging cycles, showing the power fade of the battery during aging. The estimated SOH_R matches with the measured SOH_R with MAE of 1.70%.

In order to validate the stability and reliability of the PSO-based SOH estimation algorithm in real-life applications, we added sensor noise of 5 mA and 5 mV to current and voltage data of the battery cell during the whole lifetime, respectively. The estimated capacity under sensor noise, C'_N, and estimated ohmic resistance under sensor noise, R'_0, are summarized in Table 3 and Table 4. The estimated SOH_C and SOH_R under sensor noise are depicted in Fig. 11(e) and (f), respectively. The MAEs of the estimation of capacity fade and power fade under noise are 0.89% and 2.3%, respectively, as summarized in Table 5, which demonstrates that the SOH estimation algorithm can provide accurate information of both capacity and power fade even under sensor noise.

With the experimental validation, it is evident that the proposed

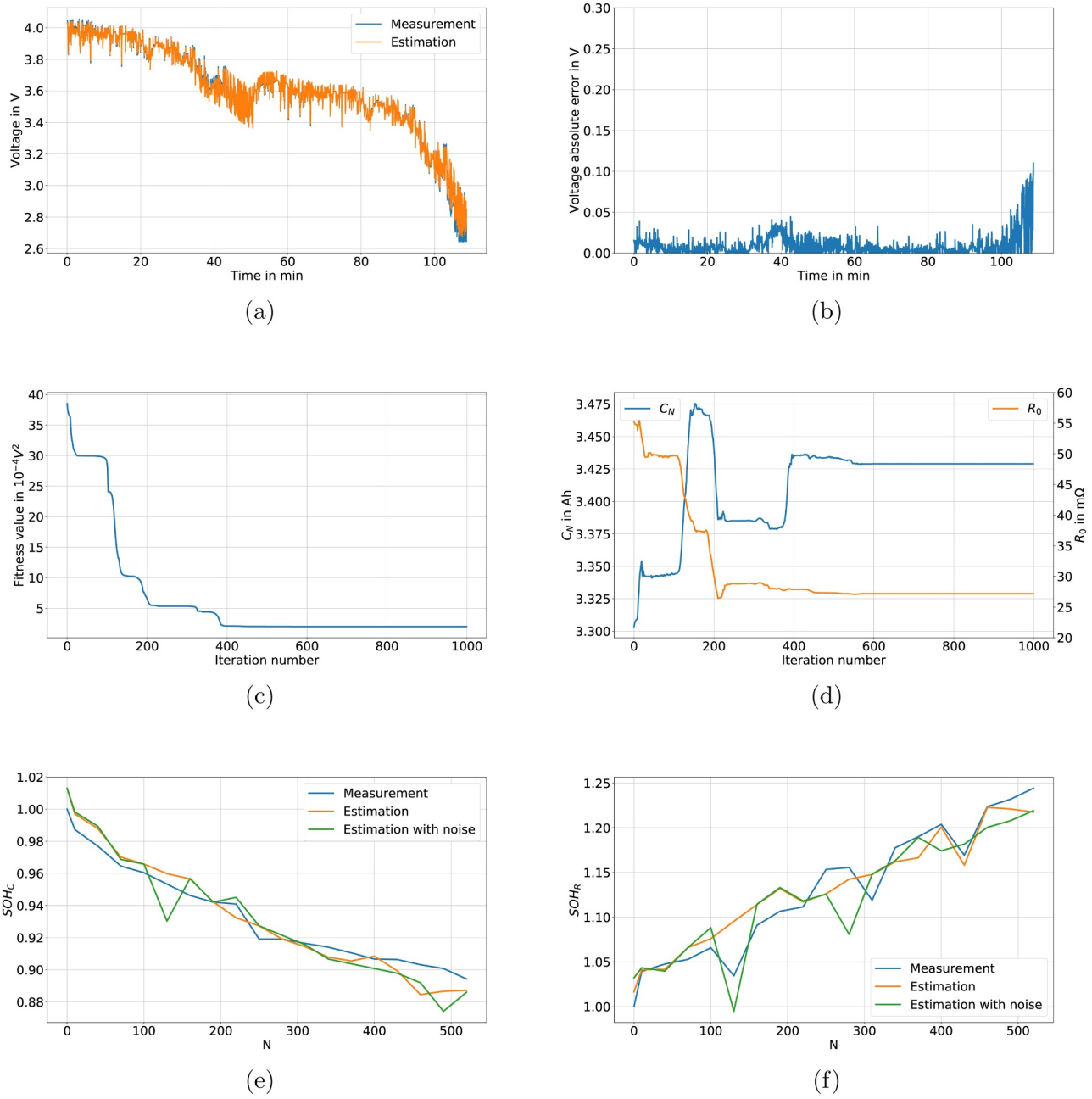

Fig. 11. Validation results of the PSO-based SOH estimation algorithm. (a) Validation results of the battery voltage estimation with the parameters estimated by PSO at BoL. (b) The absolute error of voltage estimation with the parameters estimated by PSO at BoL. (c) Convergence performance of the fitness value for the battery at BoL. (d) Convergence performance of the capacity and ohmic resistance for the battery at BoL. (e) Measurement and estimates of SOH_C with and without sensor noise during the aging test. (f) Measurement and estimates of SOH_R with and without during the aging test.

Table 3
List of cell capacity degradation index C_C, C_N and C'_N during cell aging, where C_C is the measured cell capacity with 0.33 C discharging in characterization test, C_N and C'_N are the estimates of the SOH algorithm without and with sensor noise, respectively.

Cycle number	0	10	40	70	100	130	160	190	220	250	280	310	340	370	400	430	460	490	520
C_C [Ah]	3.39	3.34	3.31	3.27	3.25	3.23	3.20	3.19	3.19	3.11	3.11	3.10	3.09	3.08	3.07	3.07	3.06	3.05	3.03
C_N [Ah]	3.43	3.38	3.35	3.29	3.27	3.25	3.24	3.19	3.16	3.14	3.11	3.10	3.07	3.07	3.08	3.05	3.00	3.00	3.01
C'_N [Ah]	3.43	3.38	3.35	3.28	3.27	3.15	3.24	3.19	3.20	3.14	3.12	3.10	3.07	3.06	3.05	3.04	3.02	2.96	3.00

PSO-based SOH estimation algorithm can provide precise information of both capacity fade and power fade of the battery in real-life applications under sensor noise, highlighting its application potential. The limitation of the proposed approach is the relatively high computation burden because of the iterated simulation of the battery model. However, the ultra-high computation and data storage capabilities of the proposed cloud BMS is able to implement this advanced SOH algorithm and open the window into the battery's capacity and power

Table 4
List of cell impedance degradation index R_C, R_0 and R_0' during cell aging, where R_C is the measured cell ohmic resistance with 2 C current pulse at 80% SOC in characterization test, R_0 and R_0' are the estimates of the SOH algorithm without and with sensor noise, respectively.

Cycle number	0	10	40	70	100	130	160	190	220	250	280	310	340	370	400	430	460	490	520
R_C [$m\Omega$]	26.7	27.8	28.0	28.2	28.5	27.7	29.2	29.6	29.7	30.8	30.9	29.9	31.5	31.8	32.2	31.3	32.7	32.9	33.3
R_0 [$m\Omega$]	27.2	27.8	27.9	28.5	28.8	29.3	29.8	30.3	29.9	30.1	30.6	30.7	31.1	31.2	32.1	31.0	32.7	32.7	32.6
R_0' [$m\Omega$]	27.6	27.9	27.8	28.5	29.1	26.6	29.8	30.3	29.9	30.1	28.9	30.7	31.1	31.8	31.4	31.6	32.1	32.3	32.6

Table 5
Comparison of the MAE of SOH estimation with and without sensor noise, where SOH_C and SOH_R are estimates without sensor noise, and SOH_C' and SOH_R' are estimates with sensor noise.

	SOH_C	SOH_C'	SOH_R	SOH_R'
MAE [%]	0.74	0.89	1.70	2.30

fade synchronously, which can be further used to take actions to optimize the operation scenarios, enhance the battery's performance and extend their service lives.

8. Conclusions

A cloud battery management system was developed based on the concept of the Internet of Things and cloud computing in this work to build up the digital twin for battery systems in the cloud and improve the computation power, data storage capability, and reliability of the BMS. We believe that this is the first exploration in the development of the digital twin for battery systems and shows both the system technical details and the operation results of the cloud-suited battery diagnostic algorithms, which is a big step to bring digital twin from theory to real industrial application. Furthermore, SOC and SOH estimation algorithms were developed based on an extended Thevenin model with AEHF and PSO, respectively, for accurate monitoring and diagnostics with the cloud BMS. This is also the first work providing both capacity fade and power fade of the battery synchronously with the PSO under dynamic operation load. The system functionalities and diagnostic algorithms were validated with the cloud BMS prototypes under field operation and experimentally with both lithium-ion and lead-acid batteries. In future work, machine learning algorithms will be developed based on the collected data from the battery systems in the cloud for precise lifetime prediction and system optimization purposes.

CRediT authorship contribution statement

Weihan Li: Conceptualization, Methodology, Software, Validation, Investigation, Writing - original draft, Writing - review & editing, Visualization. **Monika Rentemeister:** Resources, Writing - review & editing. **Julia Badeda:** Conceptualization, Validation, Writing - review & editing. **Dominik Jöst:** Resources, Validation, Writing - review & editing. **Dominik Schulte:** Resources, Writing - review & editing. **Dirk Uwe Sauer:** Conceptualization, Writing - review & editing, Supervision, Funding acquisition.

Declaration of Competing Interest

The authors declare that they have no known competing financial interests or personal relationships that could have appeared to influence the work reported in this paper.

Acknowledgment

This work was supported within the project BSMS by the European EFRE program [grant number EU-1-1-081] and within the project EVERLASTING from the Horizon 2020 program by the European Union [grant number EVERLASTING-713771]. The authors would like to thank Voltia a.s. for the real-world driving profile, Patrick Borycka from BatterieIngenieure GmbH for his contributing work and support at hardware design, and Erik Brmmendorf from aedifion GmbH for his support at the cloud platform. Thanks are also given to Decheng Cao, Ruilin Li and Iskender Demir for their support at simulation works.

Supplementary materials

Supplementary data associated with this article can be found, in the online version, at 10.1016/j.est.2020.101557.

References

[1] Y. Nishi, Lithium ion secondary batteries; past 10 years and the future, J. Power Sources 100 (1–2) (2001) 101–106, https://doi.org/10.1016/S0378-7753(01)00887-4.
[2] M. Lelie, T. Braun, M. Knips, H. Nordmann, F. Ringbeck, H. Zappen, D. Sauer, Battery management system hardware concepts: an overview, Appl. Sci. 8 (4) (2018) 534, https://doi.org/10.3390/app8040534.
[3] S. Piller, M. Perrin, A. Jossen, Methods for state-of-charge determination and their applications, J. Power Sources 96 (1) (2001) 113–120, https://doi.org/10.1016/S0378-7753(01)00560-2.
[4] S. Lee, J. Kim, J. Lee, B.H. Cho, State-of-charge and capacity estimation of lithium-ion battery using a new open-circuit voltage versus state-of-charge, J. Power Sources 185 (2) (2008) 1367–1373, https://doi.org/10.1016/j.jpowsour.2008.08.103.
[5] J. Badeda, M. Kwiecien, D. Schulte, T. Ruwald, D.U. Sauer, Adaptive battery steering and management system for the optimized operation of stationary battery energy storage systems in multi-use applications, in: I.I.T.E. Conference (Ed.), Driving innovation in ICT energy infrastructure, IEEE, [Piscataway, NJ], 2017, pp. 287–293, , https://doi.org/10.1109/INTLEC.2017.8214149.
[6] M. Kwiecien, J. Badeda, M. Huck, K. Komut, D. Duman, D. Sauer, Determination of SoH of lead-acid batteries by electrochemical impedance spectroscopy, Appl. Sci. 8 (6) (2018) 873, https://doi.org/10.3390/app8060873.
[7] W. Waag, S. Käbitz, D.U. Sauer, Experimental investigation of the lithium-ion battery impedance characteristic at various conditions and aging states and its influence on the application, Appl. Energy 102 (2013) 885–897, https://doi.org/10.1016/j.apenergy.2012.09.030.
[8] P. Shafiei Sabet, D.U. Sauer, Separation of predominant processes in electrochemical impedance spectra of lithium-ion batteries with nickel-manganese-cobalt cathodes, J. Power Sources 425 (2019) 121–129, https://doi.org/10.1016/j.jpowsour.2019.03.068.
[9] G.L. Plett, Sigma-point Kalman filtering for battery management systems of LiPB-based HEV battery packs, J. Power Sources 161 (2) (2006) 1356–1368, https://doi.org/10.1016/j.jpowsour.2006.06.003.
[10] H. He, R. Xiong, H. Guo, Online estimation of model parameters and state-of-charge of LiFePO4 batteries in electric vehicles, Appl. Energy 89 (1) (2012) 413–420, https://doi.org/10.1016/j.apenergy.2011.08.005.
[11] M. Charkhgard, M.H. Zarif, Design of adaptive h ∞ filter for implementing on state-of-charge estimation based on battery state-of-charge-varying modelling, IET Power Electron. 8 (10) (2015) 1825–1833, https://doi.org/10.1049/iet-pel.2014.0523.
[12] Y. Zhang, R. Xiong, H. He, W. Shen, Lithium-ion battery pack state of charge and state of energy estimation algorithms using a hardware-in-the-loop validation, IEEE Trans. Power Electron. 32 (6) (2017) 4421–4431, https://doi.org/10.1109/TPEL.2016.2603229.
[13] W. Waag, C. Fleischer, D.U. Sauer, Critical review of the methods for monitoring of lithium-ion batteries in electric and hybrid vehicles, J. Power Sources 258 (2014) 321–339, https://doi.org/10.1016/j.jpowsour.2014.02.064.
[14] D. Andre, C. Appel, T. Soczka-Guth, D.U. Sauer, Advanced mathematical methods of SOC and SOH estimation for lithium-ion batteries, J. Power Sources 224 (2013) 20–27, https://doi.org/10.1016/j.jpowsour.2012.10.001.
[15] J. Remmlinger, M. Buchholz, M. Meiler, P. Bernreuter, K. Dietmayer, State-of-health monitoring of lithium-ion batteries in electric vehicles by on-board internal resistance estimation, J. Power Sources 196 (12) (2011) 5357–5363, https://doi.org/10.1016/j.jpowsour.2010.08.035.
[16] D.H. Zhang, G.R. Zhu, J. Bao, Y. Ma, S.J. He, S. Qiu, W. Chen, Research on parameter identification of battery model based on adaptive particle swarm

optimization algorithm, J. Comput. Theor. Nanosci. 12 (7) (2015) 1362–1367, https://doi.org/10.1166/jctn.2015.3897.
[17] J. Spillner, J. Müller, A. Schill, Creating optimal cloud storage systems, Future Gener. Comput. Syst. 29 (4) (2013) 1062–1072, https://doi.org/10.1016/j.future.2012.06.004.
[18] A. Botta, W. de Donato, V. Persico, A. Pescapé, Integration of cloud computing and internet of things: a survey, Future Gener. Comput. Syst. 56 (2016) 684–700, https://doi.org/10.1016/j.future.2015.09.021.
[19] M. Grieves, J. Vickers, Digital twin: mitigating unpredictable, undesirable emergent behavior in complex systems, in: Transdisciplinary Perspectives on Complex Systems, vol. 89, pp. 85–113.10.1007/978-3-319-38756-7_4.
[20] T. Tanizawa, T. Suzumiya, K. Ikeda, Cloud-connected battery management system supporting e-mobility, Fujitsu Sci. Tech. J. 51 (4) (2015) 27–35.
[21] K. Friansa, I.N. Haq, B.M. Santi, D. Kurniadi, E. Leksono, B. Yuliarto, Development of battery monitoring system in smart microgrid based on internet of things (IoT), Procedia Eng. 170 (2017) 482–487, https://doi.org/10.1016/j.proeng.2017.03.077.
[22] T. Kim, D. Makwana, A. Adhikaree, J. Vagdoda, Y. Lee, Cloud-based battery condition monitoring and fault diagnosis platform for large-scale lithium-ion battery energy storage systems, Energies 11 (1) (2018) 125, https://doi.org/10.3390/en11010125.
[23] T. Zeugmann, P. Poupart, J. Kennedy, X. Jin, J. Han, L. Saitta, M. Sebag, J. Peters, J.A. Bagnell, W. Daelemans, G.I. Webb, K.M. Ting, J.S. Shirabad, J. Fürnkranz, E. Hüllermeier, S. Matwin, Y. Sakakibara, P. Flener, U. Schmid, C.M. Procopiuc, N. Lachiche, Particle swarm optimization, in: C. Sammut, G.I. Webb (Eds.), Encyclopedia of Machine Learning, Springer, New York and London, 2010, pp. 760–766, , https://doi.org/10.1007/978-0-387-30164-8_630.
[24] M. Berecibar, I. Gandiaga, I. Villarreal, N. Omar, J. van Mierlo, P. van den Bossche, Critical review of state of health estimation methods of Li-ion batteries for real applications, Renew. Sustain. Energy Rev. 56 (2016) 572–587, https://doi.org/10.1016/j.rser.2015.11.042.
[25] Alexander Farmann, Dirk Uwe Sauer, Comparative study of reduced order equivalent circuit models for on-board state-of-available-power prediction of lithium-ion batteries in electric vehicles, Appl. Energy 225 (2018) 1102–1122, https://doi.org/10.1016/j.apenergy.2018.05.066.
[26] Johannes Schmalstieg, Christiane Rahe, Madeleine Ecker, Dirk Uwe Sauer, Full Cell Parameterization of a High-Power Lithium-Ion Battery for a Physico-Chemical Model: Part I. Physical and Electrochemical Parameters, J. Electrochem. Soc. 165 (16) (2018) A3799–A3810, https://doi.org/10.1149/2.0321816jes.
[27] Johannes Schmalstieg, Dirk Uwe Sauer, Full Cell Parameterization of a High-Power Lithium-Ion Battery for a Physico-Chemical Model: Part II. Thermal Parameters and Validation, J. Electrochem. Soc. 165 (16) (2018) A3811–A3819, https://doi.org/10.1149/2.0331816jes.
[28] Weihan Li, Decheng Cao, Dominik Jöst, Florian Ringbeck, Matthias Kuipers, Frie Fabian, Dirk Uwe Sauer, Parameter sensitivity analysis of electrochemical model-based battery management systems for lithium-ion batteries, Appl. Energy 269 (2020), https://doi.org/10.1016/j.apenergy.2020.115104.
[29] D. Andre, A. Nuhic, T. Soczka-Guth, D.U. Sauer, Comparative study of a structured neural network and an extended Kalman filter for state of health, Eng. Appl. Artif. Intell. 26 (3) (2013) 951–961, https://doi.org/10.1016/j.engappai.2012.09.013.
[30] Christian Fleischer, Wladislaw Waag, Ziou Bai, Dirk Uwe Sauer, On-line self-learning time forward voltage prognosis for lithium-ion batteries using adaptive neuro-fuzzy inference system, J. Power Sources 243 (2013) 728–749, https://doi.org/10.1016/j.jpowsour.2013.05.114.
[31] Kailong Liu, Xiaosong Hu, Zhongbao Wei, Yi Li, Yan Jiang, Modified Gaussian Process Regression Models for Cyclic Capacity Prediction of Lithium-Ion Batteries, IEEE Trans. Transp. Electrific. 5 (4) (2019) 1225–1236, https://doi.org/10.1109/TTE.2019.2944802.
[32] Kailong Liu, Yi Li, Xiaosong Hu, Mattin Lucu, Widanalage Dhammika Widanage, Gaussian Process Regression With Automatic Relevance Determination Kernel for Calendar Aging Prediction of Lithium-Ion Batteries, IEEE Trans. Ind. Inf. 16 (6) (2020) 3767–3777, https://doi.org/10.1109/TII.2019.2941747.